

OPEN ACCESS

Transient analysis with fast Wilson-Daubechies time-frequency transform

To cite this article: V Necula *et al* 2012 *J. Phys.: Conf. Ser.* **363** 012032

View the [article online](#) for updates and enhancements.

You may also like

- [ON SIGNALS FAINT AND SPARSE: THE ACICA ALGORITHM FOR BLIND DETRENDING OF EXOPLANETARY TRANSITS WITH LOW SIGNAL-TO-NOISE](#)
I. P. Waldmann
- [Multiple cycles of magnetic activity in the Sun and Sun-like stars and their evolution](#)
Elena Aleksandrovna Bruevich, Vasily Vladimirovich Bruevich and Boris Pavlovich Artamonov
- [Wavelet analysis for ground penetrating radar applications: a case study](#)
Mehdi Javadi and Hasan Ghasemzadeh



ECS
The
Electrochemical
Society
Advancing solid state &
electrochemical science & technology

DISCOVER
how sustainability
intersects with
electrochemistry & solid
state science research

Transient analysis with fast Wilson-Daubechies time-frequency transform

V Necula, S Klimenko and G Mitselmakher

University of Florida, P.O.Box 118440, Gainesville, Florida, 32611, USA

Abstract. The time-frequency transforms are important tools for identification of transient events in the output of the gravitational-wave detectors. Produced by the terrestrial and possibly by astrophysical sources, the transient events can be identified as patterns on the time-frequency plane with the excess power above stationary detector noise. In this paper we consider a particular case of the Wilson-Daubechies time-frequency transform for use in the gravitational-wave burst analysis. The presented Wilson-Daubechies basis shares some properties with the Gabor frames, but circumvents the Balian-Low theorem. It also shares similarity with the Meyer wavelet, which is actively used in the gravitational-wave burst analysis. The main advantages of the Wilson-Daubechies transform are the low computational cost, spectral leakage control, flexible structure of the frequency sub-bands, and the existence of the analytic time-delay filters, which are important for localization of the gravitational-wave sources in the sky. These properties of the Wilson-Daubechies transform may prove useful not only in the transient analysis, but also in other areas of the gravitational wave data analysis and detector characterization.

1. Introduction

Time-frequency (TF) analysis is a part of searches for gravitational wave burst signals expected to accompany collapses of massive stars, mergers of compact binary objects (consisting of neutron stars and black holes), gamma ray bursts and other energetic phenomena. Such searches [1, 2, 3, 4, 5, 6, 7, 8, 9, 10, 11] have been already conducted using the data collected with the first generation ground based laser interferometer detectors (LIGO [12], VIRGO [13], GEO [14]), but no detection has been reported. The second generation detectors will start operation after 2015 with the order of magnitude better sensitivities, and the hunt for burst signals will be resumed with increased chances of success. To maximize the discovery potential of the second generation detectors, the development of new more advanced data analysis techniques is also required [15]. This paper presents a time-frequency transform first considered by Wilson [16] and detailed by Daubechies et al. [17] which can significantly improve the performance of the burst search algorithms.

Optimal matched filter techniques are not always suitable for the burst searches because for some transient GW signals accurate waveforms are not available or difficult to obtain. Also, transient events due to environmental and instrumental disturbances need to be identified in the detector data streams for a better understanding of the non-stationary noise (detector characterization). Therefore, the existing burst algorithms exploit the localization of transient events in the TF domain. With an appropriate TF basis, it is anticipated that transient events (both GW bursts and environmental disturbances) can be identified as patterns (clusters) on

the TF plane. The size, shape and the statistical properties of the clusters greatly depend on the TF transform used in the analysis.

One common approach to the burst TF analysis is to use Gabor bases (windowed Fourier) and their variations [18, 19, 20, 21, 22], where template waveforms densely cover a TF plane to produce an overcomplete representation of the data. Such TF transforms are convenient for the visualization of burst events, however their template waveforms do not form an orthogonal basis. This significantly complicates the reconstruction of burst signals, which are usually represented by multiple template waveforms. In this case, the inverse transform usually is not defined and the time domain GW signal can not be reconstructed from the TF data.

Another approach to the TF analysis is to project the data on a local orthonormal basis of wavelet functions [23]. In this case, the data in the TF domain is critically sampled (the same number of data samples before and after the transformation), the energy is conserved, the inverse transform is well defined, and the statistical independence of the TF data samples ensures a straightforward application of the clustering algorithms [24] and the coherent network reconstruction methods [25]. For example, one of the baseline LIGO-Virgo burst algorithms [26] uses Meyer's wavelet which has replaced older implementations of the TF transform based on the Symlet or Daubechies wavelets [24].

The TF transform presented in this paper combines advantages of the conventional Wilson-Daubechies transform and the Meyer wavelet. It has a better performance in several areas including: a) fast transformation by using the Fast Fourier Transform (FFT), b) shorter transformation filters (time localization), and c) better control over the spectral leakage (frequency localization). Also it offers a simple analytic expression for the time delay filters used to time-shift TF series. These filters are necessary for the sky-localization algorithms [26], which should synchronize the TF data streams from different detectors for an anticipated sky location of the GW source.

2. Wilson-Daubechies orthonormal basis

Conventional approaches to the time-frequency analysis include the windowed Fourier transform

$$\tilde{x}(\omega, t) = \int e^{-i\omega\tau} \phi(\tau - t) x(\tau) d\tau, \quad (1)$$

with ϕ as the window function, and its discrete version in frequency ω and time t based on Gabor frames

$$g_{nm}(t) = e^{im\omega \frac{t}{T}} \phi(t - nT) \quad , \quad n, m \in \mathbb{N}, \quad (2)$$

where the free parameter T defines the time resolution. In principle, with a careful choice of the window function an orthonormal basis can be constructed. However, it is a subject to the Balian-Low theorem stating that the basis functions are non-local in either time or frequency:

$$\int t^2 |\phi(t)|^2 dt = \infty \quad \text{or} \quad \int \omega^2 |\tilde{\phi}(\omega)|^2 d\omega = \infty \quad (3)$$

Wilson [16] circumvented the limitations of the Balian-Low theorem by introducing a general alternative to Gabor frames where each frequency band has its own window function. Daubechies and collaborators [17] showed that one can build a simple orthonormal Wilson basis by using just one window function $\phi(t)$ and construct the basis as:

$$g_{n0}(t) = \phi(t - nT) \quad (4)$$

$$g_{nm}(t) = \sqrt{2} (-1)^{mn} \cos(2\pi mt/T) \phi(t - nT/2) \quad , \quad m + n = 2k \quad , \quad m > 0 \quad (5)$$

$$g_{nm}(t) = \sqrt{2} \sin(2\pi mt/T) \phi(t - nT/2) \quad , \quad m + n = 2k + 1 \quad , \quad m > 0 \quad (6)$$

Also the window function should satisfy the condition

$$\sum_{l \in \mathbb{Z}} \tilde{\phi}(\omega + 2\pi l) \tilde{\phi}(\omega + 2\pi l + 4\pi m) = (2\pi)^{-1} \delta_{m0} . \quad (7)$$

There are constructions of ϕ which guarantee exponential decay in both time and frequency [17]. But in this paper we will focus on a special case where ϕ is a generalization of the Meyer wavelet scaling function, which is compactly supported in the frequency domain and decays faster than any inverse polynomial in the time domain. This choice is particularly convenient in applications to band-limited (sampled) signals because a fast discrete version of the transform can be obtained.

3. Fast Wilson-Daubechies-Meyer transform

In this section we consider a discrete data $x[k]$ sampled at the frequency r_s with the maximum angular frequency $\Omega = \pi r_s$, and find the discrete Wilson-Daubechies-Meyer (WDM) filters $f_{nm}[k]$ used to obtain the time-frequency representation of the signal:

$$w_{nm} = \sum_k f_{nm}[k] x[k] \quad (8)$$

The WDM basis functions in the Fourier domain are given by

$$\tilde{g}_{n0}(\omega) = e^{-in\omega T} \tilde{\phi}(\omega) \quad (9)$$

$$\tilde{g}_{nm}(\omega) = \frac{1}{\sqrt{2}} e^{-in\omega T/2} \tilde{\psi}_{nm}(\omega). \quad (10)$$

The exponential factors describe the time translation of the basis and the functions $\tilde{\psi}_{nm}(\omega)$ are constructed from the frequency-shifted $\tilde{\phi}(\omega)$ functions

$$\tilde{\psi}_{nm}(\omega) = C_{m+n}^* \tilde{\phi}(\omega + m\Delta\Omega) + C_{m+n} \tilde{\phi}(\omega - m\Delta\Omega) , \quad m > 0 \quad (11)$$

$$\Delta\Omega = 2\pi/T , \quad C_{2k} = 1 , \quad C_{2k+1} = i . \quad (12)$$

The generalized Meyer scaling function $\tilde{\phi}(\omega)$ is defined as

$$\tilde{\phi}(\omega) = \frac{1}{\sqrt{\Delta\Omega}} , \quad |\omega| < A \quad (13)$$

$$\tilde{\phi}(\omega) = \frac{1}{\sqrt{\Delta\Omega}} \cos \left[\nu_n \left(\frac{|\omega| - A}{B} \right) \frac{\pi}{2} \right] , \quad A \leq |\omega| < A + B , \quad (14)$$

where A and B are two positive parameters

$$2A + B = \Delta\Omega , \quad (15)$$

and $\nu_n : [0, 1] \rightarrow \mathbb{R}$ is a monotonically increasing function constructed from the incomplete Beta function $B(x; a, b)$

$$\nu_n(x) = \frac{B(x; n, n)}{B(1; n, n)} , \quad B(x; a, b) = \int_0^x t^{a-1} (1-t)^{b-1} dt . \quad (16)$$

The parameter n defines how sharp are the edges of the scaling function. For example, Figure 1 shows the two scaling functions with $n = 2$ and $n = 4$ (top plots) and their time domain counterpart (bottom plots).

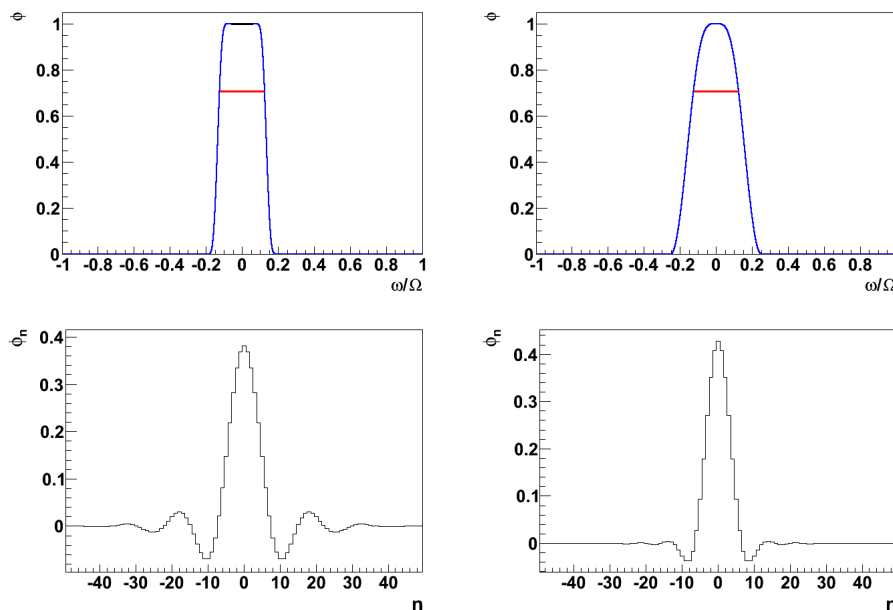


Figure 1. The top plots show $\phi(\omega)$ and highlight the defining parameters: the width of the top flat region (black) is $2A$, the transition regions (blue) are defined by B , and the red line spans the nominal band width $2A+B$. The shape of the transition region depends on the parameter n in ν_n ; $n=4$ for the left plot and $n=2$ for the right plot. The bottom plots show the coefficients of their discrete time domain representation. In these examples $M=4$ (see Equation (17)).

Only those functions \tilde{g}_{nm} which span the data frequency band $[-\Omega, \Omega]$ are relevant for the transformation. Therefore $m \leq M$, where the parameter M is given by

$$M = \frac{\Omega}{\Delta\Omega} = \frac{T}{2\tau} \quad (17)$$

and $\tau = 1/r_s$. Unless M is a natural number, the filters $f_{nm}[k]$ for $n \neq 0$ are not discrete translations of $f_{0m}[k]$, therefore $M \in \mathbb{N}$. In this case we can also redefine the functions \tilde{g}_{nM} to be

$$\tilde{g}_{nM}(\omega) = e^{-i(2n+q)M\omega\tau} \left[\tilde{\phi}(\omega + \Omega) + \tilde{\phi}(\omega - \Omega) \right] \quad , \quad |\omega| \leq \Omega \quad (18)$$

where $q = 0$, if M is even, and $q = 1$ otherwise. The new set \tilde{g}_{nm} ($0 \leq m \leq M$) forms an orthonormal basis on $[-\Omega, \Omega]$ and the explicit WDM expansion is

$$w_{n0} = \tau \sum_{k \in \mathbb{Z}} x[2nM + k] \phi[k] \quad (19)$$

$$w_{nm} = \tau \sqrt{2\Re} C_{m+n} \sum_{k \in \mathbb{Z}} e^{i\pi km/M} x[nM + k] \phi[k] \quad , \quad 0 < m < M \quad (20)$$

$$w_{nM} = \tau \sum_{k \in \mathbb{Z}} (-1)^k x[2nM + qM + k] \phi[k] \quad (21)$$

where $\phi[k]$ are the sampled values of $\phi(t)$ - the time domain representation of $\tilde{\phi}(\omega)$. Note, the Fourier inverse of $\tilde{\phi}(\omega)$ does not have a compact support in the time domain, therefore, the filter

$\phi[k]$ should be truncated. As the result the transformation is approximately orthonormal, but for any practical application the error introduced by the truncation can be made insignificant.

The formula for $0 < m < M$ case also cover both $m = 0$ and $m = M$ cases up to the normalization factor $\sqrt{2}$ and picking only the odd or even coefficients as appropriate. Therefore, using the periodicity of the exponential factor we can rewrite

$$\sum_{j=0}^{j<2M} e^{i2\pi jm/2M} X_n[j] = \sum_{k \in \mathbb{Z}} e^{i\pi km/M} x[nM + k] \phi_k \quad (22)$$

$$X_n[j] = \sum_{k \in \mathbb{Z}} x[nM + 2kM + j] \phi[2kM + j] \quad (23)$$

The data vectors X_n have the length of $2M$, and the summation on the left side of Equation (22) is the discrete Fourier transform of X_n . Therefore, the FFT algorithm can be used to speed up the calculations. The construction of the inverse transform is straightforward and also uses the FFT algorithm.

Only half of the Fourier components obtained from the vectors X_n represents the WDM expansion in Equations (19-21). The other half is the WDM expansion

$$\hat{w}_{n0} = \tau \sum_{k \in \mathbb{Z}} x[(2n + 1)M + k] \phi[k] , \quad (24)$$

$$\hat{w}_{nm} = \tau \sqrt{2} \mathfrak{S} C_{m+n} \sum_{k \in \mathbb{Z}} e^{i\pi km/M} x[nM + k] \phi[k] \quad , \quad 0 < m < M , \quad (25)$$

$$\hat{w}_{nM} = \tau \sum_{k \in \mathbb{Z}} (-1)^k x[2nM + (1 - q)M + k] \phi[k] , \quad (26)$$

in the complementary orthonormal basis constructed from the time-shifted (by $T/2$) WDM basis functions in Equations (9) and (10). Each WDM set (w_{nm} or \hat{w}_{nm}) gives a complete TF representation of the data. For $0 < m < M$ the coefficients \hat{w}_{nm} represent the quadrature of the data w_{nm} in the WDM domain. The quadrature is often used in the transient analysis and obtained with the fast WDM transform at no additional computational cost.

4. WDM time-delay filters

In the coherent analysis of data from multiple detectors, the relative time delays between detectors need to be introduced in order to synchronize the expected signal with respect to a particular source location in the sky. Time-delay filters perform this operation in the time-frequency domain and in this section we present these filters for the Wilson-Daubechies-Meyer transform.

A time shifted data $w_{nm}(\delta t)$ in the TF domain can be calculated as

$$w_{nm}(\delta t) = \sum_{lk} w_{lk} \int_{-\infty}^{\infty} g_{nm}(t + \delta t) g_{lk}(t) dt . \quad (27)$$

where w_{lk} is the original TF data. time-delay filter can be evaluated in the Fourier domain

$$\int_{-\infty}^{\infty} g_{nm}(t + \delta t) g_{lk}(t) dt = \int_{-\Omega}^{\Omega} e^{-i\omega \delta t} \tilde{g}_{nm}^*(\omega) \tilde{g}_{lk}(\omega) d\omega \quad (28)$$

Unless $|m - k| \leq 1$, the integral vanishes because there is no overlap between the basis functions. The results take a simpler form, if the time shift δt is a multiple of the sampling interval τ . Evaluating the integral one finds

$$\int g_{nm}(t + \delta t)g_{n+l,m}(t)dt = (-1)^{ln}\Re C_l^* e^{im\Delta\Omega\delta t} T_l , \quad (29)$$

$$T_l = \int_{-\Omega}^{\Omega} e^{i\omega(Ml\tau+\delta t)}|\tilde{\phi}(\omega)|^2 d\omega , \quad (30)$$

$$\int g_{nm}(t + \delta t)g_{n+l,m\pm 1}(t)dt = (-1)^{m+n}(-1)^{ln}\Re C_{l+1}^* e^{i(m\pm 1/2)\Delta\Omega\delta t}(\pm i)^l T'_l , \quad (31)$$

$$T'_l = \int_{-\Omega}^{\Omega} e^{i\omega(Ml\tau+\delta t)}\tilde{\phi}^*(\omega - \Delta\Omega/2)\tilde{\phi}(\omega + \Delta\Omega/2) d\omega . \quad (32)$$

Equation (31) has to be multiplied by $\sqrt{2}$ whenever the sub-band index (m or $m \pm 1$) is equal to 0 or M . For the WDM transform the calculation of the time-delay filters is essentially reduced to computing the integrals T_l and T_l^\pm . For comparison, for Meyer wavelet [26] the time-delay filters should be evaluated and stored for each frequency band.

5. Properties of the WDM transform

5.1. WDM as a band-pass filter

Similar to wavelets the WDM transform is representing a set of band-pass filters. Figure 2 (top plot) shows an example of the sub-band structure of the basis functions for $M = 16$. For the WDM transform presented in the paper, the first and the last WDM sub-bands cover half of the frequency resolution, however a transform with the uniform frequency resolution can be also constructed. For comparison, Fig. 2 (bottom plot) also shows the sub-band structure for the binary wavelet transform [24] which is less regular, each sub-band (frequency layer) having a different shape due to the iterative nature of the wavelet decomposition. Although, both transforms can be used for the TF representation of data, the WDM transform offers a more accurate separation of the data spectral components.

5.2. Time-frequency maps

Each data sample w_{nm} can be presented as a time-frequency pixel with dimensions $\Delta\Omega \times T/2$. Respectively, the w_{nm} can be presented as a pixel map showing the TF content of the data. Figure 3 shows the energy (w_{nm}^2) time-frequency maps for a GW signal from a merger of non-spinning binary black holes with $M_1 = M_2 = 10M_\odot$ and at distance of 10 Mpc. The WDM map (top left) shows the average energy of the signal and its quadrature, which produces a more clear signature of the signal and highlights the utility of the quadrature coefficients. The other three TF maps are obtained with different wavelet transforms. Except for the Daubechies wavelet (bottom left), which has poor TF localization due to its non-symmetric filter, the other wavelet representations are fairly similar to the WDM map. However, the wavelets are limited to $M = 2^i$ by their iterative decomposition procedure and cumbersome to use for large M .

5.3. Spectral density estimation

The WDM transform is an excellent tool for the power spectral density (PSD) estimation. Figure 4 shows the noise spectral density amplitude obtained with the PSD estimators based on the WDM ($M = 8192$, $K = 2M$, $P = 12$, $n = 7$) and windowed FFT (Hann) for one hour of data collected by the LIGO Livingston detector. In both cases the frequency resolution is 1 Hz. There is a very good agreement between the WDM and FFT in the quasi-white noise regions (around 130 Hz and 170 Hz), but the WDM transform offers a lower spectral leakage in regions dominated by the 60 Hz power line (and its harmonics) and the violin modes between 330 Hz - 350 Hz. Within the filter truncation errors, the PSD obtained with the WDM transform is

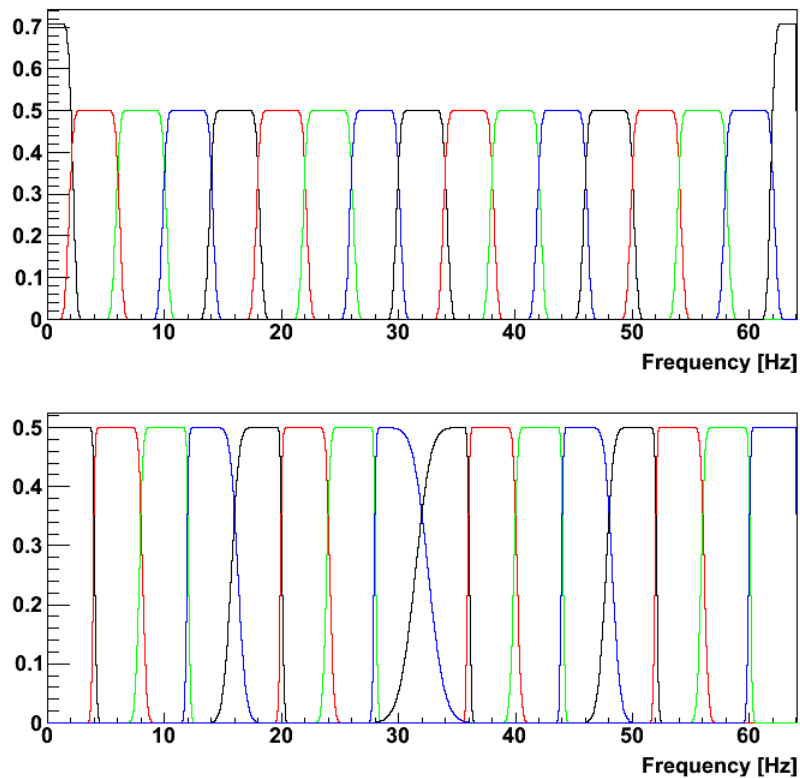


Figure 2. Spectral Fourier amplitudes of the basis functions for WDM transform (top) and binary Meyer wavelet (bottom).

an accurate representation of the data, while the windowed FFT is always altering the data by using a window in order to diminish spectral leakage.

5.4. Computational accuracy

The WDM transform is uniquely characterized by the parameters M, K

$$2A + B = \frac{\Omega}{M} \quad , \quad B = \frac{\Omega}{K} \quad , \quad K \geq M \quad (33)$$

and n from $\nu_n(x)$ defining the smooth edge of the window function. Since the time domain WDM basis functions are not compactly supported, in practice, they have to be truncated. Namely, the filter $\phi[k]$ is defined for $-L \leq k \leq L$, where $2L + 1$ is the filter length. The truncation introduces an error in the normalization of the basis functions, which can be characterized by the precision parameter

$$P = -\log_{10} \left(1 - \sum_{k=-L}^L \phi^2[k] \right) . \quad (34)$$

For a given n , ratio K/M and the precision parameter P , the filter length is proportional to M . Figure 5 shows the ratio $(2L + 1)/M$ as a function of K/M and different values of the n and P parameters.

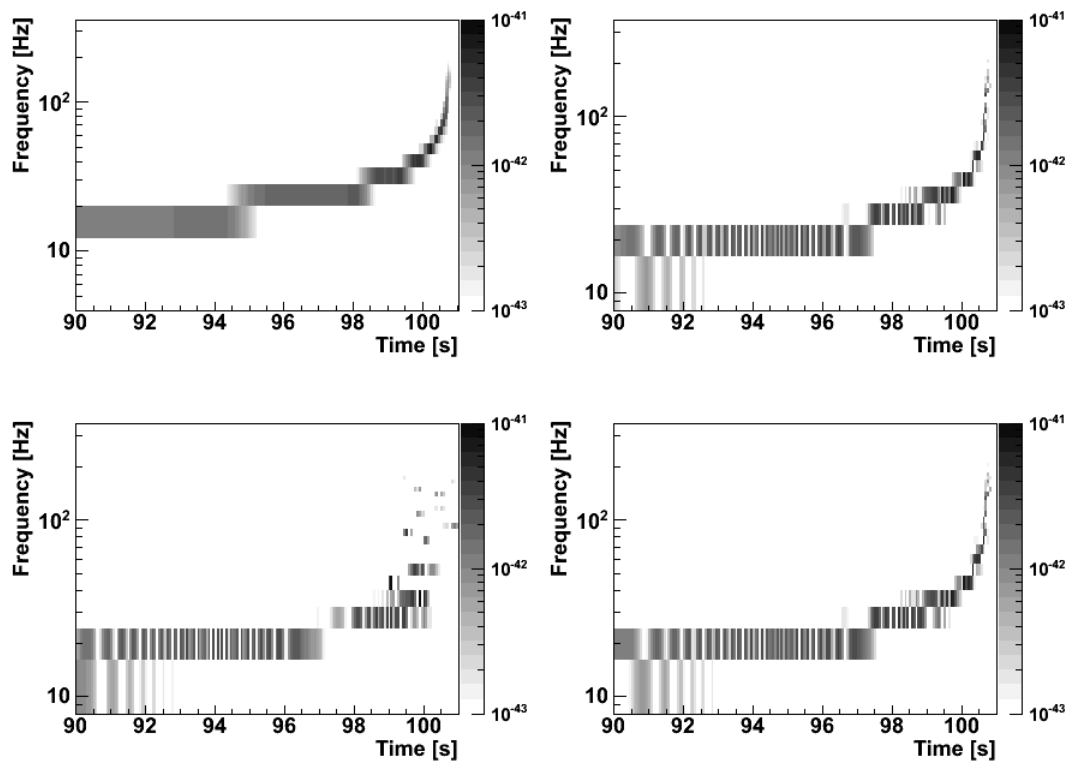


Figure 3. WDM transform (top left), Meyer (top right), Daubechies (bottom left) and Symlet (bottom right) wavelet time-frequency energy maps for a binary black hole inspiral signal.

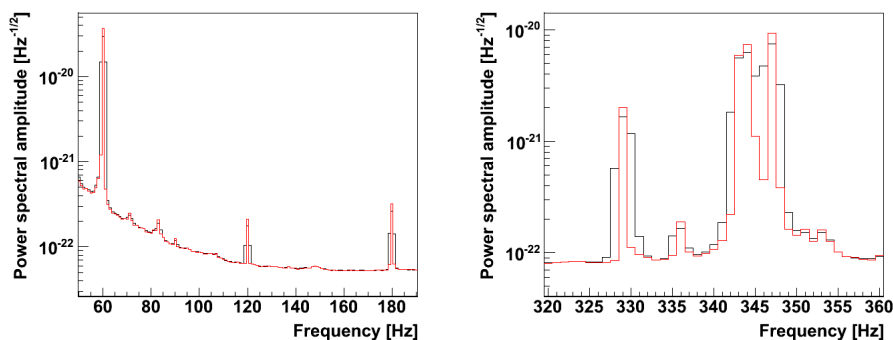


Figure 4. Spectral density amplitudes for LIGO Livingston data (GPS range 816260809 - 816264750) obtained with the WDM transform (red) and Hann windowed FFT (black).

When the n value increases, initially the filter length decreases. But for higher n the filter length starts to increase again, because in the limit $n \rightarrow \infty$ the $\phi(t)$ converges to the *sinc* function with a slowly time decay.

Another way to estimate the accuracy of the transform is to perform the forward and inverse transformations and subtract the resulting time series from the original one. Figure 6 shows the distribution of the residual data for $n = 4$, $M = 64$ and $K/M = 2$ when the input data is a

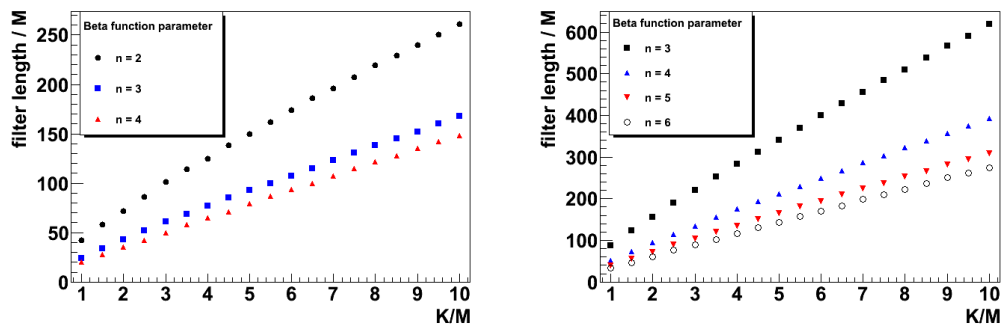


Figure 5. The ratio $(2L + 1)/M$ as a function of K/M for different values of the Beta function parameter n and two precision requirements: $P = 8$ (left) and $P = 12$ (right)

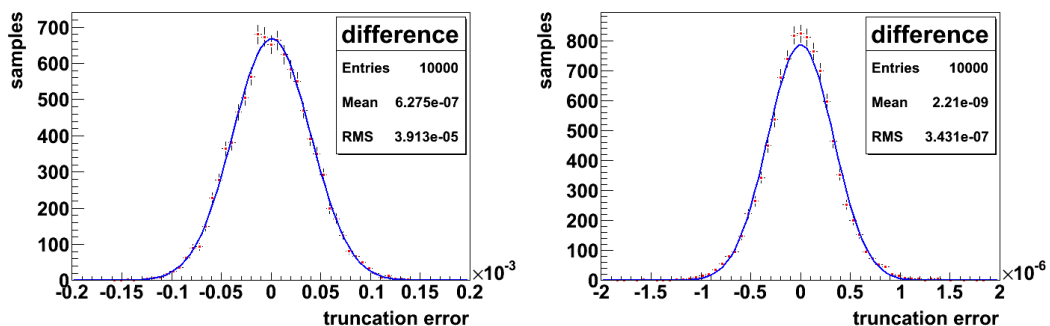


Figure 6. Truncation errors for the inverse/forward transformation ($n = 4, M = 64, K/M = 2$) of white Gaussian noise with the unity variance: $P = 8$ (left) and $P = 12$ (right).

white Gaussian noise with the unity variance.

5.5. Accuracy of the time delay filters

Truncation of $\phi[k]$ also affects the time-delay filters. By using the integrals T_l and T'_l (Eq. 30,32), they need to be constructed for every WDM frequency band m and the time-delay parameter δt . For a given m and δt , the achieved precision (calculated similar to Eq. 34 with the sum taken over the time-delay filter coefficients) of the time-delay transformation depends on the number of the filter coefficients (filter length L_{TD}). Figure 7 (left plot) shows the precision as a function of the sub-band index m and the delay index $\delta t/\tau$ for $L_{TD} = 123$. By selecting the central point ($m = \delta t/\tau = 32$) as a conservative representation of the precision of all filters, the filter length can be estimated as a function of $K/M, n$ and P (see Fig. 8).

Acceptable accuracy of the time-delay transformation can be achieved for $L_{TD} > 60$. Figure 7 (right plot) shows the difference between the time-delay transformation ($L_{TD} = 123$ and $\delta t/\tau = 32$) implemented in the WDM domain and the correct values obtained with the WDM transform ($M = 64, K = 2M, n = 3$) of the delayed data in the time domain, which is a white Gaussian noise with the unity variance.

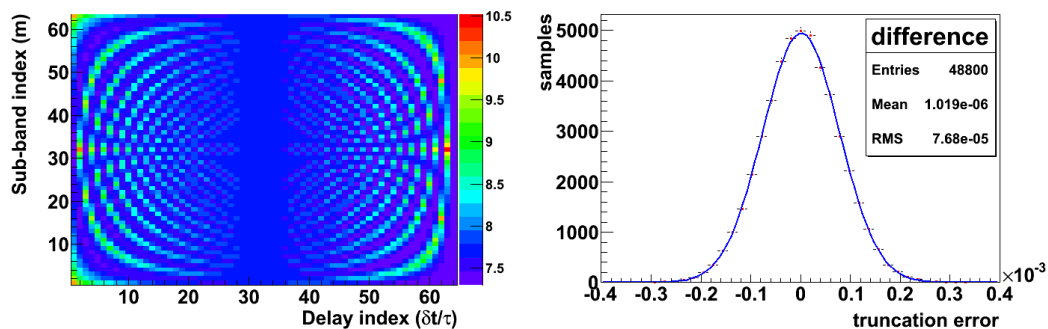


Figure 7. The left plot shows time delay filters precision with truncation at $L_{TD}=123$ for $M=64$, $K=2M$, $n=3$. The right plot shows the time-delay filter truncation errors for Gaussian noise with unity variance.

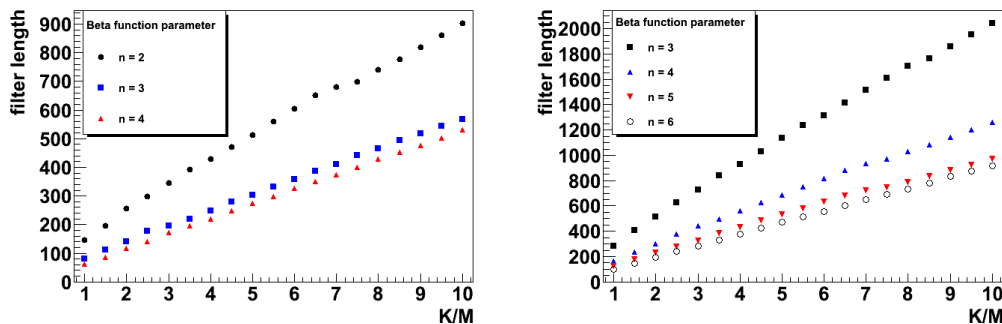


Figure 8. Time-delay filter length (L_{TD}) as a function of K/M and n for two different precision requirements, $P = 8$ (left) and $P = 12$ (right)

5.6. Complexity

Let N be the number of samples in the time series, and M, K, P the parameters defining the transformation. The number of multiplications needed to obtain the TF data is

$$C_{WDM} = 2N \left[\log_2 2M + \frac{L(K, M, P)}{M} \right] \quad (35)$$

where $2L(K, M, P) + 1$ is the length of the WDM filter. The first term in square parenthesis represents the complexity of the FFT and the second term is the added complexity due to the multiplication by the WDM filter (per 1/2 data sample). For comparison, the windowed FFT performed with the 50% overlap between the adjacent windows has a complexity

$$C_{FFT} = 2N [\log_2 M + 1] . \quad (36)$$

The FFT is always faster, but for large M the computational performance of the WDM transform becomes comparable. The complexity of the binary wavelet transform is

$$C_W = N L_W \log_2 M , \quad (37)$$

where L_W is the wavelet filter length. It is comparable with the FFT only for Haar wavelet ($L_W = 2$). For longer wavelet filters ($L_W \sim 1000$), required to reduce spectral leakage, the

computational cost of the wavelet transform is significantly higher than for the FFT and the WDM.

6. Conclusion

The fast discrete Wilson-Daubechies-Meyer (WDM) transform is a promising tool for the gravitational-wave burst analysis. With the WDM transform the transient events can be efficiently localized on the TF plane. The transform is orthonormal and critically sampled, which significantly simplifies the statistical analysis in the TF domain. The conservation of energy is approximate, however, for any practical application the transformation errors can be made insignificant. Depending on the particular requirements of the analysis, the transform's parameters (M , K , n and P) can be customized to optimize the performance. Analytic time delay filters are readily available to perform time-shifts of data directly in the TF domain. The inverse transform is also available. These properties of the WDM transform make it a convenient tool for the coherent network analysis and the reconstruction of the GW waveforms and source coordinates. Due to a superior spectral leakage control, the WDM transform provides an accurate spectral density estimation which can be particularly useful for monitoring of a quasi-stationary noise typical for real detectors. With its unique properties, the WDM transform may prove useful not only for burst searches, but also in the other areas of the gravitational wave data analysis and detector characterization.

7. Acknowledgements

This work was supported by the US National Science Foundation grants PHY-0855044 and PHY-0855313 to the University of Florida, Gainesville, Florida.

References

- [1] Abbott B *et al* 2004 *Phys. Rev. D* **69** 102001
- [2] Abbott B *et al* 2005 *Phys. Rev. D* **72** 062001
- [3] Abbott B *et al* 2005 *Phys. Rev. D* **72** 122004
- [4] Abbott B *et al* 2006 *Class. Quantum Grav.* **23** S29
- [5] Abbott B *et al* 2007 *Class. Quantum Grav.* **24** 5343
- [6] Abbot B P *et al* 2009 *Phys. Rev. D* **80** 102001
- [7] Abbot B P *et al* 2010 *Astrophys. J.* **715** 1438
- [8] Abadie J *et al* 2010 *Phys. Rev. D* **81** 102001
- [9] Abbott B *et al* 2008 *Phys. Rev. Lett.* **101** 211102
- [10] Abbot B P *et al* 2009 *Astrophys. J.* **701** L68
- [11] Abadie J *et al* 2011 *Astrophys. J.* **734** L35
- [12] Abbott B P *et al* 2009 *Rep. Prog. Phys.* **72** 076901
- [13] Acernese F *et al* 2006 *Class. Quantum Grav.* **23** S635
- [14] Luck H *et al* 2006 *Class. Quantum Grav.* **23** S71
- [15] LIGO-Virgo Collaboration, LIGO Document T1100322
<https://dcc.ligo.org/cgi-bin/DocDB/ShowDocument?docid=62893>
- [16] Wilson K G, preprint, Cornell University
- [17] Daubechies I, Jaffard S and Journé J L 1991 *J. Math. Anal.* **22** pp 554-673
- [18] Anderson W G, Brady P R, Creighton J D E and Flanagan É É 2001 *Phys. Rev. D* **63** 042003
- [19] Searle A C, Sutton P J and Tinto M 2009 *Class. Quantum Grav.* **26** 155017
- [20] Beauville F *et al* 2008 *Class. Quantum Grav.* **25** 045002
- [21] Kalmus P, Khan R, Matone L and Marka S 2007 *Class. Quantum Grav.* **24** S659
- [22] Chatterji S, Lazzarini A, Stein L, Sutton P, Searle A and Tinto M 2006 *Phys. Rev. D* **74** 082005
- [23] Daubechies I 1992 *Ten Lectures on Wavelets* (Philadelphia, PA: SIAM)
- [24] Klimenko S and Mitselmakher G, 2004 *Class. Quantum Grav.* **21** S1819
- [25] Klimenko S, Mohanty S, Rakhmanov M and Mitselmakher G 2005 *Phys. Rev. D* **72** 122002
- [26] Klimenko S, Yakushin I, Mercer A and Mitselmakher G 2008 *Class. Quantum Grav.* **25** 114029
- [27] Meyer Y 1992 *Wavelets and Operators* (Cambridge: Cambridge University Press)